Ultrasound in Med. & Biol., Vol. 29, No. 7, pp. 1027–1035, 2003

0301-5629/03/$–see front matter

ELSEVIER

doi:10.1016/S0301-5629(03)00051-6

● *Original Contribution*

BREAST CANCER DIAGNOSIS USING THREE-DIMENSIONAL ULTRASOUND AND PIXEL RELATION ANALYSIS

WEI-MING CHEN,* RUEY-FENG CHANG,* WOO KYUNG MOON† and DAR-REN CHEN‡*
*Department of Computer Science and Information Engineering, National Chung Cheng University, Chiayi, Taiwan; †Department of Diagnostic Radiology, Seoul National University Hospital, Seoul, South Korea; and ‡Department of General Surgery, China Medical College & Hospital, Taichung, Taiwan

(*Received* 29 *August* 2002; *revised* 15 *January* 2009; *in final form* 10 *February* 2003)

Abstract—Because ultrasound (US) imaging offers benefits compared with other medical imaging techniques, it is used routinely in nearly all hospitals and many clinics. However, the surface features and internal structure of a tumor are not easily demonstrated simultaneously using the traditional 2-D US. The newly developed three-dimensional (3-D) US can capture the morphology of a breast tumor and overcome the limitations of the traditional 2-D US. This study deals with pixel relation analysis techniques for use with 3-D breast US images and compares its performance to 2-D versions of the images. The 3-D US imaging was performed using a Voluson 530 scanner. The rectangular subimages of the volume-of-interest (VOI) were manually selected and the selected VOIs were outlined to include the entire extent of the tumor margin. The databases in this study included 54 malignant and 161 benign tumors. All solid nodules at US belong over C3 (probably benign) according to ACR BI-RADS category. All or some selected 2-D slices were used separately to calculate the diagnosis features for a 3-D US data set. We have proposed and compared several different methods to extract the characteristics of these consecutive 2-D images. As shown in our experiments, the diagnostic results were better than those of the conventional 2-D US. In the experiments, the area index *Az* under ROC curve of the proposed 3-D US method can achieve 0.9700 ± 0.0118, but *Az* of the 2-D US is only 0.8461 ± 0.0315. The *p* value of these two *Az* differences using z test is smaller than 0.01. Furthermore, we can find that the features from only several slices are enough to provide good diagnostic results if the adopted features are modified from the 2-D features. (E-mail: dlchen88@ms13.hinet.net) **© 2003 World Federation for Ultrasound in Medicine & Biology.**

Key Words: **3-D breast ultrasound, Pixel relation analysis, Breast tumor, Neural network.**

INTRODUCTION

Breast ultrasound (US) is routinely used as an adjunct to mammography, to help diagnose accurately whether a tumor is benign or malignant. Although several sonographic features of benign and malignant solid breast lesions have been described (Egan and Egan 1984; Leucht et al. 1988; Fornage et al. 1989; Stavros et al. 1995), a significant number of breast masses may still not demonstrate a typical sonographic appearance. Recently, significant technical advances were made in diagnostic sonography. For example, higher frequency linear transducers were introduced. The high computing power of sonography platforms can allow fully digital systems, and this digitization is of great help in computer applications for image processing. This higher quality of US images makes for greater development and utilization of image pixel relation analysis. The works by Chen et al. (1999, 2000a, 2000b) have demonstrated the potential of pixel relation analysis for computer-aided diagnostic (CAD) algorithms. Similar applications have been reported for other types of medical images (Wei et al. 1995; Morishita et al. 1995; Ito et al. 1995; Petrick et al. 1996; Vittitoe et al. 1997). In the studies of Chen and collegues, the benign and malignant tumors were classified by using a 5×5 normalized autocorrelation matrix, and a multilayer feed-forward neural network was used to perform the diagnostic task.

On many areas of current US development, none is of greater interest than three-dimensional (3-D) US (Nelson et al. 1999). 3-D US exploits the real-time capability to build a volume that can then be explored using the power of modern computer workstations. Currently, the 3-D US systems adopt mechanical, freehand and 2-D array scanning techniques (Nelson et al. 1999; Fenster et

Address correspondence to: Prof. Dar-Ren Chen, Department of General Surgery, China Medical College & Hospital, 2 Yer-Der Rd, Taichung, Taiwan. E-mail: dlchen88@ms13.hinet.net

Table 1. The number of tumors for various specific types in this study

Benign (n = 107)			Malignant (n = 54)			
Fibroadenoma	Fibrocystic nodule	Other	Invasive ductal carcinoma	Intraductal carcinoma	Lobular carcinoma	Mucinous carcinoma
51	52	4	49	2	1	2

al. 2001). Recently, the speckle decorrelation technique has been applied to provide image-based registration, which allows accurate 3-D volume rendering (Tuthill et al. 1998). One of the advantages of 3-D US is that it can well represent the morphology of an organ of interest, such as in the field of echocardiography and obstetrics. A recent study of 3-D breast US showed that it can provide transverse longitudinal planes, as well as simultaneously the coronal plane. This additional information has been proven to be helpful for clinical applications (Rotten et al. 1999). Reports (Rankin et al. 1993; Fenster and Downey 1996; Downey et al. 2000; Fenster et al. 2001) have shown that 3-D US has advantages over conventional 2-D techniques. There are many 3-D US applications, such as the diagnosis of breast masses (Rotten et al. 1999) and core needle breast biopsy (Weismann et al. 2000; Smith et al. 2001).

To represent the pixel relation information of a tumor, all US slices for a tumor should be used. However, in the traditional 2-D CAD system, only a slice is used to extract the pixel relation information (Chen et al. 1999, 2000a, 2000b). The pixel relation information from only one slice may fail to represent all the pixel relation information of a tumor. Hence, the accuracy of 2-D US image analysis may be affected by the transducer position during image acquisition, and the operator must be able to control the transducer position to identify the relevant structures and locations. We believe that 3-D US will overcome the limitations of conventional 2-D US. Here, we will present several approaches modified from the traditional 2-D approach for all slices or only some selected slices of 3-D US based on the pixel relation features.

MATERIALS AND METHODS

Data acquisition

A radiologist (Moon WK) supplied all the 3-D US data sets. Data sets were collected from January 2001 to June 2001, and all supplied cases were used for analysis without selection. The database contained 161 pathologically proven breast tumors, including 107 benign and 54 malignant tumors. The range of tumor sizes was from 0.51 cm to 3.54 cm in diameter. All solid nodules at US belong over C3, according to ACR BI-RADS category. That is, all indeterminate cases correspond to BI-RADS category C4 (suspicious). The "benign" category corresponds to ACR BI-RADS category C3 (probably benign) and "malignant" corresponds to C5 (highly suggestive of malignancy). Most of the cases were in the category of indeterminate or malignant, because we included only histologically confirmed cases. Table 1 lists the number of tumors for various specific types in this study.

The 3-D US imaging was performed using a Voluson 530 (Kretz Technik, Zipf, Austria) scanner and a Voluson small part transducer S-VNW5 to 10. The transducer, which is a linear-array transducer with a frequency of 5 to 10 MHz, a scan width of 40 mm (switchable in 3-mm steps) and a sweep angle of 20 to 25°, allows the performance of a 3-D volume scan. The patient was in the supine position with arm extended overhead and no stand-off pad was used. The lesion of interest was focused after 2-D examination was completed; then it was analyzed with 3-D breast US. The volume data were saved into a computer file on a magneto-optical (MO) disk. The MO file could be read and analyzed in a personal computer.

The rectangular subimages of the volume-of-interest (VOI) were manually selected by a breast surgeon (Chen DR) who is experienced with 3-D breast US interpretations and CAD applications, but unfamiliar with the tissue diagnosis and cell type before the VOI selections. The selected VOIs were outlined to include the entire extent of the tumor margin.

Autocorrelation function

Due to the artefacts of speckle noise and some existing low-intensity regions, such as blood vessels, it is difficult to extract the features from the US images by a common image-processing technique (Cheng et al. 1997b). The pixels in the tumor having a lower level intensity than the surrounding normal tissue is a general breast tumor feature (Cheng et al. 1997a). Chen et al. (1999) suggested that the 2-D normalized autocorrelation coefficients are suitable to reflect the interpixel relations within an image and make it possible to differentiate benign and malignant breast masses. Different tissues have significantly different pixel relations in US images.

Benign tumors are classically described as regular masses with homogeneous internal echoes, but carcinomas are described as having fuzzy borders with heterogeneous internal echoes. The correlation between neighboring pixels within the 2-D images is a patent feature of the tumor. This study is based on the pixel relation analysis techniques developed by Chen et al. (1999, 2000a, 2000b). In their technique, the normalized autocorrelation coefficients are used to reflect the interpixel correlation within an image, and the normalized autocorrelation coefficients can be defined as:

$$\gamma(\Delta m,\Delta n) = \frac{A(\Delta m,\Delta n)}{A(0,0)}, \quad (1)$$

where

$$A(\Delta m,\Delta n) = \frac{1}{(M-\Delta m)(N-\Delta n)} \times \sum_{x=0}^{M-1-\Delta m} \sum_{y=0}^{N-1-\Delta n} f(x,y) f(x+\Delta m, y+\Delta n), \quad (2)$$

where $\gamma(\Delta m, \Delta n)$ is the normalized autocorrelation coefficient between pixel (x, y) and pixel $(x + \Delta m, y + \Delta n)$ in an image with size $M \times N$.

To generate similar autocorrelation features for images with different brightness but with a similar pixel relation, the autocorrelation coefficients are further modified into mean-removed autocovariance coefficients. This autocovariance is expressed as

$$\gamma(\Delta m,\Delta n) = \frac{A'(\Delta m,\Delta n)}{A'(0,0)}, \quad (3)$$

where

$$A'(\Delta m,\Delta n) = \frac{1}{(M-\Delta m)(N-\Delta n)} \times \sum_{x=0}^{M-1-\Delta m} \sum_{y=0}^{N-1-\Delta n} |(f(x, y) - \bar{f})(f(x+\Delta m, y+\Delta n) - \bar{f})|, \quad (4)$$

and $\bar{f}$ is the mean value of $f(x, y)$. The absolute value is adopted in the above equation because a negative value may be produced when the grey level of a pixel is subtracted from the mean. In this study, these autocovariance coefficients for each breast tumor US image are found and used as interpixel pixel relation features to distinguish the differences between benign and malignant tumors.

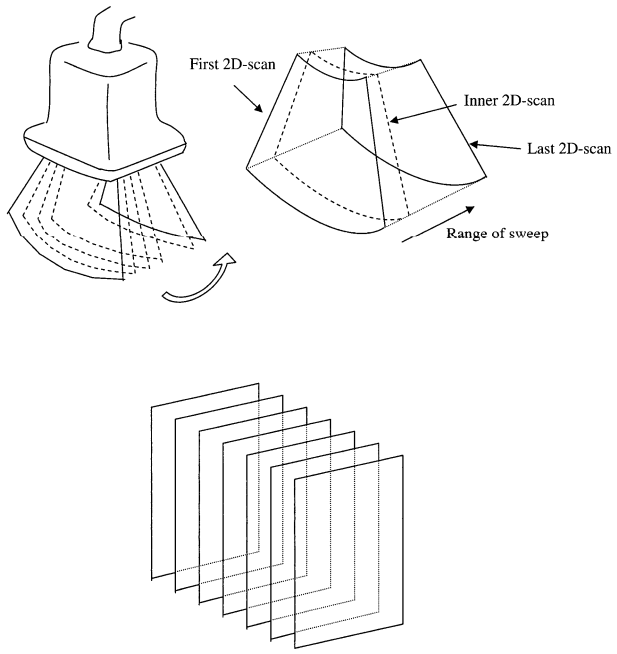

Fig. 1. (a) 3-D volume transducer. (b) 3-D US data in Cartesian coordinates.

The 3-D US images were obtained through the reconstruction of the 2-D planes scanned by the 3-D volume transducer. Because the 2-D image planes are arranged in a fanlike geometry, these scanned planes are not parallel to each other, as shown in Fig. 1a. The reconstructing program must rearrange the pixels of the fanlike image planes into a set of consecutive 2-D image planes in Cartesian coordinates, as shown in Fig. 1b. This transformation to Cartesian coordinates can be done by the Voluson 530D.

In general, the pixel rates (in pixels per cm) of each 3-D US image are not all the same and are decided by the magnifier control. In practice, the range of pixel rates in our database was between 20.35 pixels/cm and 110.56 pixels/cm. For an US image, the autocorrelation calculation will generate a 5×5 autocorrelation matrix. Because the large variation of the resolution will affect and reduce the diagnostic result, the distances Δm and Δn in the autocorrelation matrix should not be fixed for all cases and should be changed according to their the pixel rates. The calibrated expression is defined as:

$$\Delta m = \Delta n = \lfloor \text{Pixel\_Rate} \times \text{Skip\_Step} \rfloor \quad (5)$$

where the units of the Pixel_Rate and Skip_Step are pixels/cm and cm, respectively. In this work, the value of the Skip_Step is 0.018 cm.

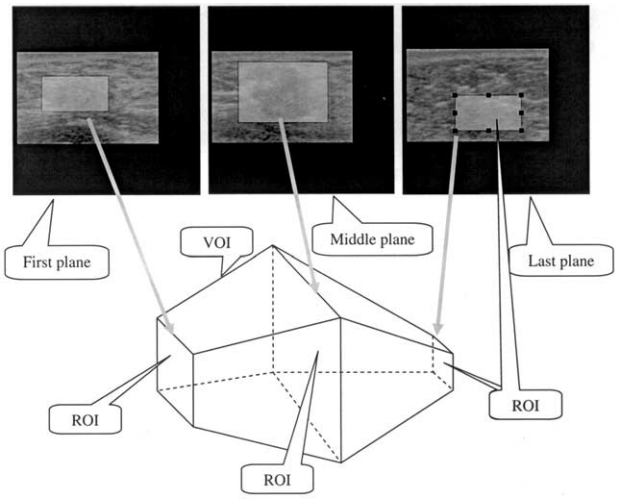

Fig. 2. The flow chart of the scheme using accumulative auto-correlation matrix.

Autocorrelation schemes for 3-D US images

With the 3-D US, the scanned slices are reconstructed into a single 3-D volume data. The original 2-D autocorrelation coefficients do not accord with the 3-D volume data set. To overcome this problem, we propose three new feature extraction methods to reduce the dimension of 3-D volume data from three to two to fit the 2-D extraction function and attempt to compare the diagnostic result of these methods later.

Accumulative autocorrelation matrix

The first method is called the accumulative autocorrelation scheme (ACC-US). In the scheme, each 2-D image is first extracted from a 3-D volume data set and then the pixel relation coefficients are computed for each 2-D image. Let the autocorrelation matrix for 3-D data set i be A^i. These coefficients of 2-D images will be accumulated into a new autocorrelation matrix A_{ACC}. Each element $A_{ACC}(m,n)$ can be computed by:

$$A_{ACC}(m,n) = \sum_i A^i(m,n). \quad (6)$$

The accumulative matrixes for all the 3-D training data sets are then fed into the neural network to compete the training process; then, the trained neural network could be used for breast tumor diagnosis. Figure 2 shows the flow chart of the pixel relation analysis technique for the 3-D US, based on the ACC matrix. There are two main stages. In the first segmentation stage, the extraction of VOI is carried out and the ACC matrix is computed. The procedure of VOI extraction is carried out in two steps. First, the physician must decide three key planes in the 3-D volume, called the first, middle and last planes. As

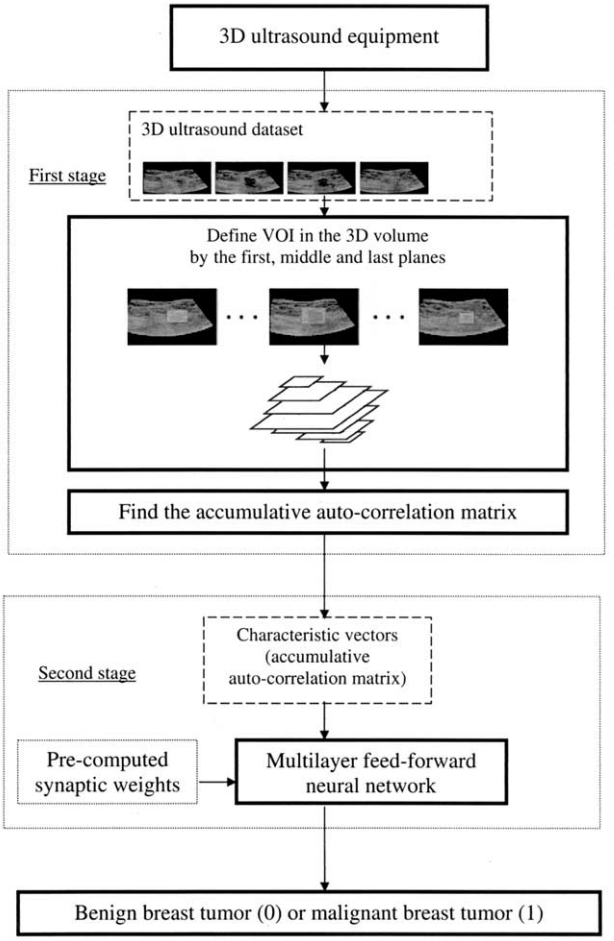

Fig. 3. The VOI defined by the three key ROIs.

shown in Fig. 3, the first plane is the first slice that contains the tumor and the last plane is the last slice that contains tumor. The middle plane is the slice where the area of tumor is biggest. Second, the physician needs to define three regions-of-interest (ROIs) in these three planes, respectively. The proposed system then uses the linear interpolation method to decide the ROIs of other planes in the 3-D volume by three key ROIs and, then, all the ROI are combined to form a VOI. After the VOI is extracted, the ACC matrix may be computed and used as a characteristic vector.In the second stage, the characteristic vectors of the training tumors will be fed into the input layer of the neural network and start the learning process. In this study, a relatively simple feed-forward, error back-propagation artificial neural network (ANN) with one hidden layer was adopted. The output of each ANN will be a number between zero and one.

Multiple autocorrelation matrixes

In the above, the coefficient matrix of each 2-D image within a 3-D US data set will be calculated and

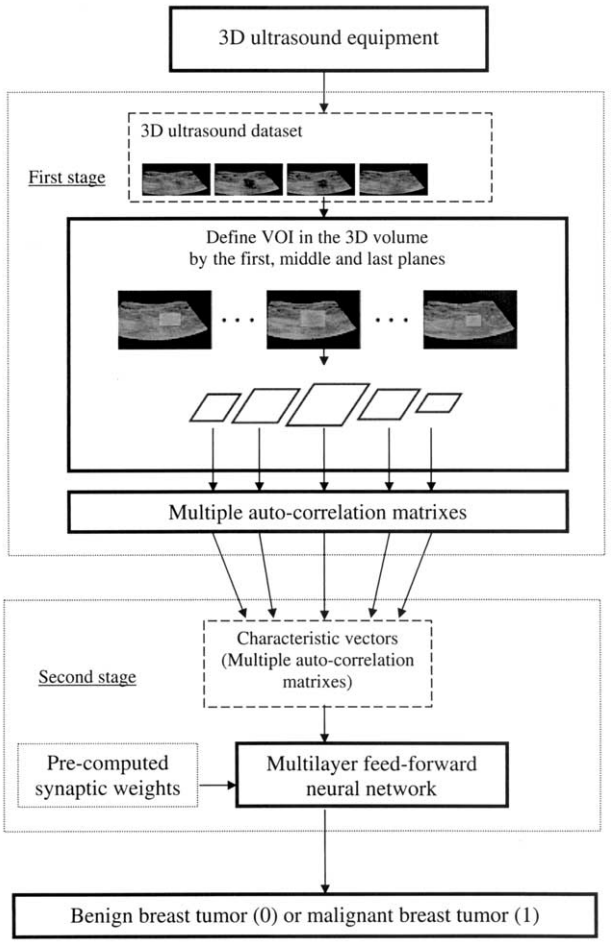

Fig. 4. The flow chart of the 2-D multiple autocorrelation scheme.

added into an ACC coefficient matrix. The pixel relation characteristic of tissues may be lost by such an accumulative operation and result in a false diagnosis. To improve the diagnostic accuracy, another pixel relation feature extraction scheme is proposed. This scheme of multiple autocorrelation matrixes (MULTI-US) explores more than one autocorrelation matrix for keeping the coefficients of each 2-D image in the 3-D volume. Because the number of frames in a 3-D volume data set is large, it is impossible to use all the coefficient matrixes. Hence, only five matrixes were used to reduce the computation time. Let *mid* be the number of the middle frame of the VOI and its autocorrelation matrix be A^{mid}. Then, the five matrixes A^{mid-2}, A^{mid-1}, A^{mid}, A^{mid+1} and A^{mid+2} for the neighboring frames $mid-2$, $mid-1$, $mid+1$, $mid+2$ of the middle frame will be used as the characteristic matrixes in the pixel relation analysis. Also, the diagnostic model needs to be modified to fit multiple coefficient matrixes.

The diagram of the proposed system is shown in Fig. 4. In the first stage, the VOI extraction method is just like the previous scheme; however, the ACC matrix is replaced by using five autocorrelation matrixes. Next, the five autocorrelation matrixes are fed into the neural network. In the second stage, the diagnosis method is modified. Each matrix is fed into the neural network and five neural network outputs will be obtained. These diagnosis outputs need to be combined into a final diagnostic output. In this study, if over two diagnostic outputs were malignant, then the final diagnosis result was malignant.

Accumulative autocorrelation matrix with only five frames

The third scheme is a combination of the above two schemes. That is, the five matrixes of the second scheme are added into an accumulative matrix. The method can not only reduce the computation time of the first scheme, but also avoid too many ROIs to influence the feature extraction result, because some ROIs may contain incomplete pixel relation information on the tumor. The hybrid scheme is called an ACC matrix with five frames (ACC5-US). The element $A_{ACC5}(m,n)$ of accumulative matrix is defined as:

$$A_{ACC5}(m,n) = A^{mid-2}(m,n) + A^{mid-1}(m,n) + A^{mid}(m,n) + A^{mid+1}(m,n) + A^{mid+2}(m,n).$$

Table 2. The number of malignant and benign tumors, number of iterations and error distortions in each training set for ACC5-US and CN-US schemes

			n Iterations		Error distortions	
Training set	*n* Malignant	*n* Benign	ACC5-US	CN-US	ACC5-US	CN-US
1,2,3,4,5	54	107	20,000	20,000	7.7210	12.8795
1,2,3,4	44	84	14,298	20,000	0.4697	9.4330
1,2,3,5	43	86	13,007	20,000	0.4954	8.7985
1,2,4,5	43	86	18,813	20,000	0.4962	7.0472
1,3,4,5	43	86	13,695	20,000	0.4998	6.4470
2,3,4,5	43	86	20,000	20,000	6.2373	9.0362

Table 3. The performance of neural network for different threshold values

Threshold	True negatives	True positives	False-negatives	False-positives	Sensitivity	Specificity
Accumulative autocorrelation matrix						
1.0	107	0	54	0	0	1
0.9	0	0	17	7	0.6852	0.9345
0.8	100	38	16	7	0.7037	0.9345
0.2	94	42	12	13	0.7778	0.8785
0.1	92	45	9	15	0.8333	0.8598
0	0	54	0	107	1	0
Multiple autocorrelation matrixes						
1.0	107	0	54	0	0	1
0.9	95	31	23	12	0.5926	0.9626
0.8	95	31	23	12	0.6111	0.9626
0.2	87	42	12	20	0.7963	0.8878
0.1	87	45	9	20	0.7777	0.8878
0	0	54	0	107	1	0
Accumulative autocorrelation matrix with only five frames						
1.0	107	0	54	0	0	1
0.9	103	42	12	4	0.7778	0.9626
0.8	103	44	10	4	0.8148	0.9626
0.2	97	49	5	10	0.9074	0.9065
0.1	96	49	5	11	0.9074	0.8972
0	0	54	0	107	1	0
Conventional 2-D US method						
1.0	107	0	54	0	0	1
0.9	93	33	21	14	0.6111	0.8691
0.8	91	35	19	16	0.6481	0.8504
0.2	86	38	16	21	0.7037	0.8037
0.1	83	38	16	24	0.7037	0.7757
0	0	54	0	107	1	0

Simulations

In the experiment, the size of Δm and Δn is 5 for all cases. Each time the autocorrelation calculation will generate a 5×5 autocorrelation matrix (*i.e.,* 25 autocorrelation coefficients). Because the autocorrelation matrix is normalized, $\gamma(0, 0)$ is always 1. Thus, except for the element $\gamma(0, 0)$, other autocorrelation coefficients can be formed as a 24-dimension characteristic vector. Including the predefined threshold, the multilayer feed-forward neural network includes 25 input nodes, 10 hidden nodes and a single output node. The degree of freedoms (*i.e.,* the number of connections) is 260. The training process is stopped when the improvement of error distortion is smaller than 0.001 or when the number of training iterations is more than 20,000.

The 3-D volume database was separated into m groups. First, m-1 groups were used as training data and one group as the outside data. After the training process was stopped, the network was then tested on the outside group and the result recorded. Next, the outside group was then replaced with another group in the training sets and the training and testing operation continued again. This operation was repeated until all m groups had been used in turn as the outside group. In these three simulations, the number m of groups was five and each group had about 32 3-D volume datasets.

Furthermore, the conventional 2-D US method (Leucht et al. 1988) was also used and its performance compared with that of the proposed schemes. The ROI of the middle plane of VOI in the 3-D US data set was used in the conventional 2-D US method.

Table 4. Classification of breast nodules by the schemes using an accumulative matrix (at TH = 0.1), multiple matrices (at TH = 0.1), an accumulative matrix with five frames (at TH = 0.2), and 2-D method (at TH = 0.2)

Ultrasound classification	ACC-US		MULTI-US		ACC5-US		CN-US	
	Benign	Malignant	Benign	Malignant	Benign	Malignant	Benign	Malignant
Benign	*TN* 92	*FN* 9	*TN* 87	*FN* 9	*TN* 97	*FN* 5	*TN* 86	*FN* 16
Malignant	*FP* 15	*TP* 45	*FP* 20	*TP* 45	*FP* 10	*TP* 49	*FP* 21	*TP* 38
Total	107	54	107	54	107	54	107	54

Table 5. Classification of breast nodules by an experienced radiologist

Radiologist classification	Histology benign	Histology malignant
Benign	6	2
Indeterminate	96	13
Malignant	5	39
Total	107	54

RESULTS

Table 2 lists the number of training iterations and error distortions for ACC5-US and CN-US schemes. The error is computed by the absolute difference between the desired output and the actual output of the neural network. Table 3 lists the performance of proposal schemes for different threshold values. The best result of each scheme is listed in Table 4 for comparison. Table 5 lists the classification results by an experienced radiologist (Moon WK). Because all solid nodules at US belong over C3, according to ACR BI-RADS category, many benign cases were categorized as indeterminate. This represents the total number of lesions requiring biopsy. Table 6 and Fig. 5 illustrate the experimental results using the following measurements:

$$\text{Accuracy} = (TP + TN)/(TP + TN + FP + FN)$$

$$\text{Sensitivity} = TP/(TP + FN),$$

$$\text{Specificity} = TN/(RN + FP),$$

$$\text{Positive Predictive Value} = TP/(TP + FP)$$

$$\text{Negative Predictive Value} = TN/(TN + FN),$$

where *TN* is the number of benign case that are diagnosed correctly, *FP* is the number of benign cases that are misdiagnosed, *TP* is the number of malignant cases that are diagnosed correctly and *FN* is the number of malignant cases that are misdiagnosed.

	Accuracy	Sensitivity	Specificity	PPV	NPV
CN-US	77.02%	70.37%	80.37%	64.41%	84.31%
ACC-US	85.09%	83.33%	85.98%	75.00%	91.09%
MULTI-US	82.61%	83.33%	81.31%	69.70%	90.63%
ACC5-US	90.68%	90.74%	90.65%	83.05%	95.10%

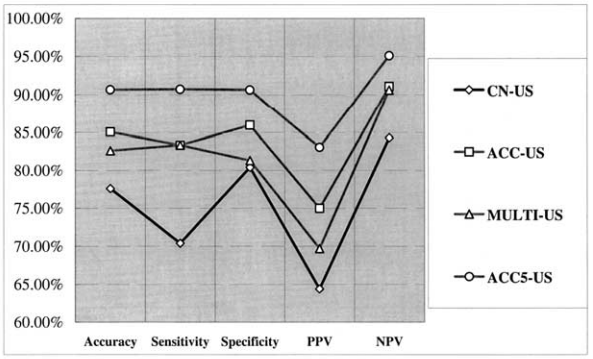

NPV: Negative Predictive Value PPV: Positive Predictive Value

Fig. 5. Comparison of the proposed and conventional schemes.

The accuracy of proposed ACC5-US scheme was 90.68% (146 of 161), the sensitivity was 90.74% (49 of 54), the specificity 90.65% (97 of 107), the positive predictive value was 83.05% (49 of 59) and the negative predictive value was 95.1% (97 of 102). In Table 6, the *p* value using χ^2 is also listed to indicate whether the difference is statistically significant or not. In Fig. 5, all the proposal schemes are superior to the conventional 2-D method. The receiver operating characteristic (ROC) curve will be used to represent the diagnostic performance In this study, the software package LABROC1 by Professor C.E. Metz, University of Chicago, is used to fit the ROC curve. Figure 6 illustrates the ROC curves for different schemes in the classification of malignant and benign tumors. The overall performance of schemes can be evaluated by examining the ROC area index, A_Z, over the diagnostic output values. The proposed ACC5-US method has a highest A_Z value of 0.9700 ± 0.0118 (SD). Table 7 lists *p* values of the difference between the areas A_z under the two ROC curves using the z-test. Only the A_z difference of MULTI-US method with the 2-D method was not statistically significant.

Table 6. Performance comparisons

Item	ACC-US	CN-US	*p* (ACC-US vs CN-US)*	MULTI-US	*p* (MULTI-US vs CN-US)*	ACC5-US	*p* (ACCS-US vs. CN-US)*
Accuracy (%)	85.09	77.02	<0.1	82.61	<0.5	90.68	<0.001
Sensitivity (%)	83.33	70.37	<0.2	83.33	<0.2	90.74	<0.01
Specificity (%)	85.98	80.37	<0.5	81.31	<1	90.65	<0.05
Positive predictive value (%)	75.00	64.41	<0.25	69.70	<1	83.05	<0.025
Negative predictive value (%)	91.09	84.31	<0.20	90.63	<0.2	95.10	<0.02

*p values using chi^2 test.

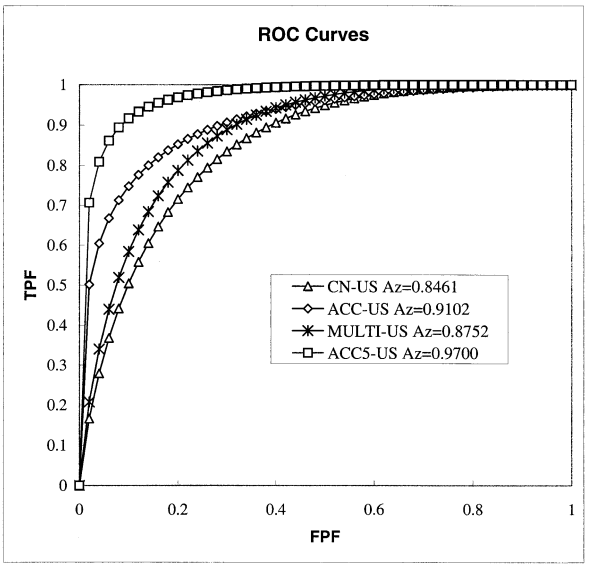

Fig. 6. The ROC curves of the various schemes for the classification of malignant and benign tumors. The A_Z value for the ROC curve of the ACC-US method is 0.9102 ± 0.0247, the A_Z value of MULTI-US method is 0.8752 ± 0.0288, the A_Z value of ACC5-US method is 0.9700 ± 0.0118 and the A_Z value of CN-US method is 0.8461 ± 0.0315.

DISCUSSION

Currently, due to the small number of test cases, the cross-validation method is adopted. Because each set was used as the test set once, five sets of parameters for neural network were used. In the future, this proposal diagnostic system should be tested using only one standard set of parameters when a large number of cases are collected.

The spiculation feature is mostly used to diagnose the breast tumors using 3-D US. In the later study by Rotten et al. (1999), the coronal section in the 3-D US allows precise demonstration of the tissue surrounding the central lesion. A converging pattern of the peripheral tissue is highly suspicious of malignancy. The converging pattern is a spiculation in which alternating hypoechoic and hyperechoic lines radiate in multiple directions from the mass into the surrounding tissue. This feature is well seen on mammograms, and malignancy cannot be excluded based on this finding. In their experiments, 91% (53 of 58) of malignant tumors and 6% (8 of 128) of benign tumors have spiculations. Although there are several successful spiculation detection techniques on mammograms (Karssemeijer and teBrake 1996; Kobatake and Yoshinaga 1996; Vyborny et al. 2000; Liu et al. 2001), the automatic spiculation detection on US images is not easily implemented due to the speckle noise in US images. Moreover, a mature segmentation algorithm is needed to segment the tumor. This study provides another way to use the 3-D US. Our method is based on the pixel relation analysis technique that is successfully implemented on the 2-D US. Because the multilayer feedforward neural network can extract higher-order statistics by adding one or more hidden layers, this model has become extremely popular in terms of classification and prediction. Hence, the multilayer feedforward neural network is adopted for classification in this paper. The computation time is rather critical on clinical applications. The proposal algorithm can use only the middle five consecutive frames in a 3-D US data set to quickly obtain the pixel relation information. That is, the proposal method can be used in real-time clinical applications.

Table 7. p value of the difference between the areas A_z under the two ROC curves using z-test

ROC curves	p value (using z test)
ACC-US and CN-US	< 0.01
MULTI-US and CN-US	< 0.5
ACC5-US and CN-US	< 0.05

Although the autocorrelation function of the ACC-US scheme is computed using all slices of 3-D US data set from a tumor, that may contain too much extra tumor tissue in the VOI so as to make a suboptimal result. Both the MULTI-US and ACC5-US schemes use only five selected slices, but the ACC5-US scheme can obtain a better result. That is, the accumulative method is effective for only some selected slices, not all slices, and can provide a more reliable diagnostic feature. The CN-US scheme uses only one slice that acts as in conventional 2-D US; its performance was the worst.

Although all the pixel relation information of a tumor is used in the first scheme using an ACC matrix, its performance is worse than that of the third scheme in which only the pixel relation information of five consecutive frames is adopted. We cannot say that the whole pixel relation information of a tumor is useless. We think that the problem is on the feature extraction method. Other advanced feature extraction methods should be further studied for the pixel relation information of all sections in a tumor.

REFERENCES

Chen DR, Chang RF, Huang YL. Computer-aided diagnosis applied to US of solid breast nodules by using neural networks. Radiology 1999;213(2):407–412.

Chen DR, Chang RF, Huang YL. Breast cancer diagnosis using self-organizing map for sonography. Ultrasound Med Biol 2000a;26(3): 405–411.

Chen DR, Chang RF, Huang YL, et al. Texture analysis of breast tumors on sonograms. Semin Ultrasound CT MR 2000b;21(4):308–316.

Cheng X-Y, Akiyama I, Itoh K, et al. Automated detection of breast tumors in ultrasonic images using fuzzy reasoning. Washington, DC: IEEE, 1997a:420–423.

Cheng X-Y, Akiyama I, Itoh K, et al. Breast tumor diagnosis system using three dimensional ultrasonic echography. In: Engineering in Medicine and Biology Society, 1997, Proceedings of the 19th Annual International Conference of the IEEE. Chicago, IL: Engineering in Medicine and Biology Society, 1997b:517–520.

Downey DB, Fenster A, Williams JC. Clinical utility of three-dimensional US. Radiographics 2000;20(2):559–571.

Egan RL, Egan KL. Automated water-path full-breast sonography: Correlation with histology of 176 solid lesions. AJR Am J Roentgenol 1984;143(3):499–507.

Fenster A, Downey DB. 3-D ultrasound imaging: A review. IEEE Eng Med Biol Mag 1996;15(6):41–51.

Fenster A, Downey DB, Cardinal HN. Three-dimensional ultrasound imaging. Phys Med Biol 2001;46(5):67–99.

Fornage BD, Lorigan JG, Andry E. Fibroadenoma of the breast: Sonographic appearance. Radiology 1989;172(3):671–675.

Ito M, Ohki M, Hayashi K, et al. Trabecular texture analysis of CT images in the relationship with spinal fracture. Radiology 1995; 194(1):55–59.

Karssemeijer N, teBrake GM. Detection of stellate distortions in mammograms. IEEE Trans Med Imaging 1996;15(5):611–619.

Kobatake H, Yoshinaga Y. Detection of spicules on mammogram based on skeleton analysis. IEEE Trans Med Imaging 1996;15(3): 235–245.

Leucht WJ, Rabe DR, Humbert KD. Diagnostic value of different interpretative criteria in real-time sonography of the breast. Ultrasound Med Biol 1988;14(Suppl. 1):59–73.

Liu S, Babbs CF, Delp EJ. Multiresolution detection of spiculated lesions in digital mammograms. IEEE Trans Image Process 2001; 10(6):874–884.

Morishita J, Doi K, Katsuragawa S, Monnier-Cholley L, MacMahon H. Computer-aided diagnosis for interstitial infiltrates in chest radiographs: Optical-density dependence of texture measures. Med Phys 1995;22(9):1515–1522.

Nelson TR, Downey DB, Pretorius DH, Fenster A. Three-dimensional ultrasound. Philadelphia, PA: Lippincott Williams & Wilkins, 1999.

Petrick N, Chan HP, Wei D, et al. Automated detection of breast masses on mammograms using adaptive contrast enhancement and texture classification. Med Phys 1996;23(10):1685–1696.

Rankin RN, Fenster A, Downey DB, et al. Three-dimensional sonographic reconstruction: Techniques and diagnostic applications. AJR Am J Roentgenol 1993;161(4):695–702.

Rotten D, Levaillant JM, Zerat L. Analysis of normal breast tissue and of solid breast masses using three-dimensional ultrasound mammography. Ultrasound Obstet Gynecol 1999;14(2):114–124.

Smith WL, Surry KJ, Mills GR, Downey DB, Fenster A. Three-dimensional ultrasound-guided core needle breast biopsy. Ultrasound Med Biol 2001;27(8):1025–1034.

Stavros AT, Thickman D, Rapp CL, et al. Solid breast nodules: Use of sonography to distinguish between benign and malignant lesions. Radiology 1995;196(1):123–134.

Tuthill TA, Krucker JF, Fowlkes JB, Carson PL. Automated three-dimensional US frame positioning computed from elevational speckle decorrelation. Radiology 1998;209(2):575–582.

Vittitoe NF, Baker JA, Floyd CE Jr. Fractal texture analysis in computer-aided diagnosis of solitary pulmonary nodules. Acad Radiol 1997;4(2):96–101.

Vyborny CJ, Doi T, O'Shaughnessy KF, et al. Breast cancer: Importance of spiculation in computer-aided detection. Radiology 2000; 215(3):703–707.

Wei D, Chan HP, Helvie MA, et al. Classification of mass and normal breast tissue on digital mammograms: Multiresolution texture analysis. Med Phys 1995;22(9):1501–1513.

Weismann CF, Forstner R, Prokop E, Rettenbacher T. Three-dimensional targeting: A new three-dimensional ultrasound technique to evaluate needle position during breast biopsy. Ultrasound Obstet Gynecol 2000;16(4):359–364.